LA-UR-15-27897 (Accepted Manuscript)

Catalytic Activity in Lithium-Treated Core–Shell MoOx/MoS2 Nanowires

Cummins, Dustin Ray; Martinez, Ulises; Kappera, Rajesh; Voiry, Damien; Martinez-Garcia, Alejandro; Jasinski, Jacek; Kelly, Daniel; Chhowalla, Manish; Mohite, Aditya; Sunkara, Mahendra; Gupta, Gautam

To be published in: The Journal of Physical Chemistry C

DOI to publisher's version: 10.1021/acs.jpcc.5b05640

Permalink to record: http://permalink.lanl.gov/object/view?what=info:lanl-repo/lareport/LA-UR-15-27897

Catalytic Activity in Lithium Treated Core-Shell MoO_x/MoS_2 Nanowires

Dustin R. Cummins[1,2], Ulises Martinez[1], Rajesh Kappera[1,3], Damien Voiry[3], Alejandro Martinez-Garcia[2], Jacek Jasinski[2], Dan Kelly[4], Manish Chhowalla[3], Aditya D. Mohite[1], Mahendra K. Sunkara[2]*, and Gautam Gupta[1]*

[1]MPA-11, Los Alamos National Laboratory, Los Alamos, NM 87545, USA

[2]Department of Chemical Engineering and Conn Center for Renewable Energy, University of Louisville, Louisville, KY 40292, USA

[3]Materials Science and Engineering, Rutgers University, Piscataway, NJ 08854, USA

[4]Chemistry Division, Chemical Diagnostics and Engineering Group, Los Alamos National Laboratory, Los Alamos, NM 87545, USA

Corresponding Authors. Gautam Gupta[a] Mahendra K. Sunkara[b]

[a]gautam@lanl.gov

[b]mahendra@louisville.edu

KEYWORDS: molybdenum disulfide, catalysis, nanowires, hydrogen evolution, intercalation

Abstract

Significant interest has grown in the development of earth abundant and efficient catalytic materials for hydrogen generation. Layered transition metal dichalcogenides present opportunities for efficient electrocatalytic systems. Here, we report the modification of 1D MoO_x/MoS_2 core-shell nanostructures by lithium intercalation and the corresponding changes in morphology, structure, and mechanism of H_2 evolution. The 1D nanowires exhibit significant improvement in H_2 evolution properties after lithiation, reducing the HER onset potential by ~50 mV and increasing the generated current density by ~600%. The high electrochemical activity in the nanowires results from disruption of MoS_2 layers in the outer shell, leading to increased activity and concentration of defect sites. This is in contrast to the typical mechanism of improved catalysis following lithium exfoliation, *i.e.* crystal phase transformation. These structural changes are verified by a combination of Raman and X-ray photoelectron spectroscopy (XPS).

1. Introduction

Hydrogen offers the potential for clean energy, but improvements in efficient and sustainable production of hydrogen fuels are required to realize its potential. Currently, 90% of hydrogen is produced from fossil resources *via* thermal steam reforming (coal and natural gas).[1-3] While alternative technologies such as water electrolysis[4] and photolytic water splitting[5] are being pursued, most of these technologies require expensive platinum and platinum based composites[6-9], which can be readily "poisoned" by chemical contaminants. Transition metal dichalcogenides (TMDs) as catalysts for the hydrogen evolution reaction (HER) provide an opportunity to address these issues.[10-31]

TMDs are earth-abundant materials with the chemical formula MX_2, in which M represents a transition metal from group IV, V or VI, and X corresponds to a chalcogen (S, Se, or Te). In particular, MoS_2 has been demonstrated to be potentially efficient catalyst for

HER.[20] Bulk MoS_2 has a hexagonal (2H-MoS_2) crystal structure with its edges being catalytically active while the basal plane is largely inactive.[18, 19, 29, 32] HER properties of several MoS_2 morphologies have been studied, including particles[16, 30], nanowires[17], double gyroid structures[19], CVD grown crystals[18], vertically oriented sheets[24-26], chemically exfoliated single layers[14, 27], joining with other TMD co-catalysts[33], and combination with carbon structures to improve conductivity.[22, 23]

For model MoS_2 structures, HER activity has been attributed to either edge sites and/or phase transformation of the basal plane.[14, 18] Extensive analysis by Chianelli, *et al*. has demonstrated that 2H-MoS_2 has a trigonal prismatic orientation, with each sulfur atom strongly bound to three Mo atoms to form the basal plane, making this surface chemically inert.[34] Any catalytic processes occur at sulfur vacancies, which are more concentrated at the edge of the crystal. These edge sites where the S-Mo dimer and S defects occur more often, have more conducting, metallic properties, compared to the bulk crystal[35] and are the preferential sites for adsorption and catalysis.[18, 36, 37]

A metastable phase of MoS_2 with a trigonal crystal structure and octahedral orientation (1T-MoS_2) has been shown to have significantly different electronic properties than the hexagonal 2H phase. 2H-MoS_2 has an indirect band gap of 1.2 eV and has semiconductor properties.[38] The bulk semiconductor can be chemically[39] or mechanically exfoliated[40]; single layers of MoS_2 exhibit a direct band gap transition of 1.9 eV. The hexagonal to trigonal phase transformation is typically achieved by intercalation of lithium between the layers, which donates an electron and creates strain in the crystal lattice.[41-44] This 1T-MoS_2 is metallic in nature[13, 45] and has high catalytic performance for HER.[14, 26-28]

In this paper, we use lithium intercalation to modify 1D core-shell MoO_x/MoS_2 nanowires, which results in an efficient HER catalyst. Core-shell MoO_x/MoS_2 nanowires have been reported previously and possess good electrocatalytic activity, however the MoS_2 shell is composed of the 2H semiconducting phase and the basal planes are oriented parallel to

the nanowire axis, possessing a lower number of active sites.[17, 20] Our results indicate that lithium intercalation disrupts the MoS_2 shell and creates numerous edge defects while maintaining the nanowire 1D morphology, which leads to increased hydrogen evolution characteristics. This destruction of ordered crystal structures has been well studied in lithium-ion battery electrode applications[46] and dramatic volume expansions have been shown during lithium intercalation of graphene, ranging from only 10% for elemental lithium to a few hundred percent increase when using lithium solvents.[47]

2. Materials and Methods.

2.1 Synthesis of Nanostructured Materials

The synthesis of MoO_3 nanowires is described in previous work.[17, 48] The sulfurization of these oxide nanowires was performed at 300°C for 2 hours in a 15 Torr 99% H_2S atmosphere. Lithium exfoliation of these nanowires, as well as the formation of the 2D sheets, was performed by soaking in n-butyl lithium for 24 hours, then heavy rinsing with DI water to fully remove the lithium. This is shown schematically in Figure S1.

2.2 Electrochemical Characterization

The rinsed nanowires are dispersed in DI water and then transferred to a glassy carbon electrode. Further, a thin layer (~2.7 μL/cm^2) of 5% Nafion solution is deposited on top of the electrode to prevent the nanowires or sheets from delaminating and to enhance proton conductivity. The HER activity is measured in 0.5 M H_2SO_4 (pH = 0) electrolyte in a three-electrode configuration with Ag/AgCl reference electrode (+0.210 V vs. RHE), graphite rod as counter electrode, and glassy carbon with or without MoS_2 nanostructures as working electrode. The electrolyte is purged with nitrogen to remove oxygen from the system. The working electrodes are subjected to initial cycling (-0.35 V to +0.2 V vs. RHE) to remove surface contamination and are cycled until a steady state is achieved prior to collection of the data. In an attempt to standardize the electrocatalytic performance, every effort is taken to ensure a similar loading of catalytic material on the electrode, both nanowires and 2D sheets.

Since the metastable 1T-MoS_2 structure is notoriously sensitive to slightly elevated temperatures[45], the active material is heated in an inert atmosphere at various temperatures for 1 hour, then allowed to cool under vacuum. The annealed material is then transferred to the glassy carbon electrode and the electrochemical testing is performed as described previously.

3. Results and Discussion

3.1 Effect of Lithiation on Nanowires and 2D Sheets

MoO_3 nanowire arrays were grown on stainless steel substrates using hot filament chemical vapor deposition (HFCVD) and exposed to H_2S[17, 48], (15 Torr 99% H_2S at 300°C). Figure 1 shows electron microscopy images of MoS_2 nanostructures before and after lithiation. Nanowires form a vertically oriented array, with diameters ranging from 20–50 nm and lengths of 1–3 μm, as seen in Figure 1A. HR-TEM imaging (Figure 1B) shows the oriented crystalline 2H-MoS_2 shell with a thickness of 5-10 nm around a single crystal MoO_x core. TEM measurements indicate that the MoS_2 shell is single crystalline across the radius of the shell, but has low angle grain boundaries along the length of the nanowire, with the basal plane of 2H-MoS_2 (100) oriented parallel to the length of the nanowire. Chemical exfoliation is performed by reacting the as-synthesized nanowires in n-butyl lithium solution for a desired time, followed by thoroughly rinsing with DI water to remove excess lithium. The lithiation and subsequent washing steps slightly disrupts and delaminates the nanowire array as a whole, which is evidenced in the SEM image Figure 1C, but the individual nanowire morphology is unchanged. Upon examination with HR-TEM, it can be readily observed that the lithium intercalation (Figure 1D) significantly disrupts the ordered crystal structure of the MoS_2 shell, leading to a polycrystalline MoS_2 shell with random orientations and increased edge defects while still maintaining the nanowire morphology. Electron energy loss spectroscopy (EELS) analysis is used to demonstrate that there is almost no lithium residue in the MoS_2 nanowires after extensive washing[15] and is reported in the Supporting Information (Figure S3). A similar procedure is used for lithiation of bulk MoS_2 powder

(Figure 1E) to form single layer 1T-MoS_2 sheets (Figure 1F). STEM analysis of the 2D sheets (Figure 1G) shows that each sheet is single crystalline with predominant phase to be 1T-MoS_2.

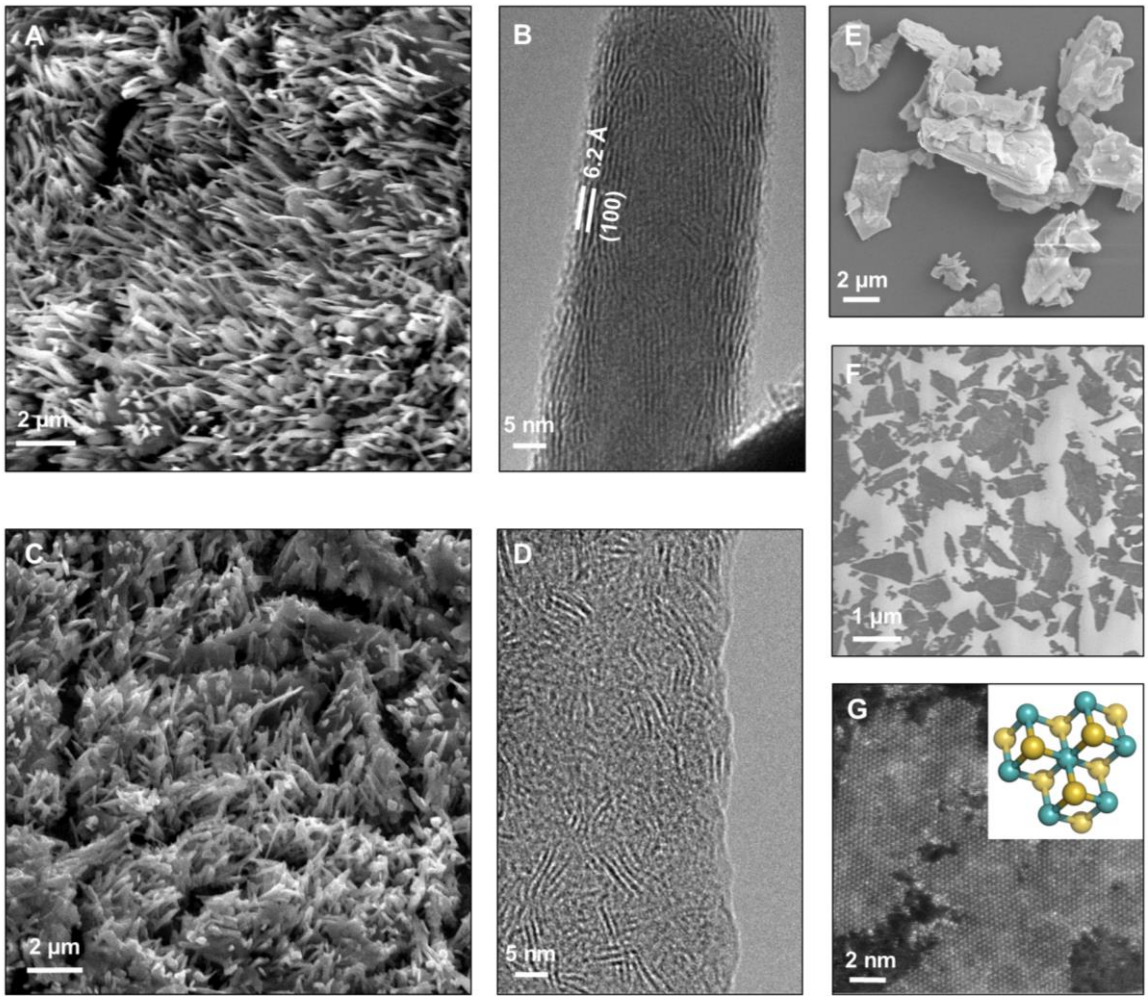

Figure 1. Micrographs of MoS_2 nanowires and sheets before and after lithiation. A) SEM image of the as-grown nanowires. B) TEM of the as-grown nanowires, showing the ordered MoS_2 shell on the MoO_x core. C) SEM of the MoS_2 nanowires after lithiation. D) TEM of the nanowires after lithiation, showing the disordered crystal shell. E) SEM of bulk 2H-MoS_2 powder. F) SEM of the lithium exfoliated MoS_2 sheets. G) STEM of the 1T flakes after lithiation, with an inset showing a molecular model of 1T-MoS_2. The 1T phase can be distinguished by STEM due to a change in contrast from the sulfur atoms. In the 2H-MoS_2 lattice, 2 sulfur atoms overlap when viewed in profile, however in the 1T phase, due to the lattice rotation, there is only one sulfur atom, which leads to the intensity of the imaged sulfur

in 2H to be twice as bright. This is explained more fully in multiple fundamental studies.[13, 15, 44]

3.2 Electrochemical Activity of Catalysts for Evolution of H_2

Electrochemical HER studies were performed to investigate the effect of lithiation. The catalytic materials were deposited (approximately 0.1 mg) on glassy carbon electrodes and electrochemical measurements were performed in 0.5 M H_2SO_4. All data is iR corrected to account for resistance inherent in the testing system (~12 Ω); the Nyquist plot showing the series resistance is reported in the Supporting Information (Figure S4).

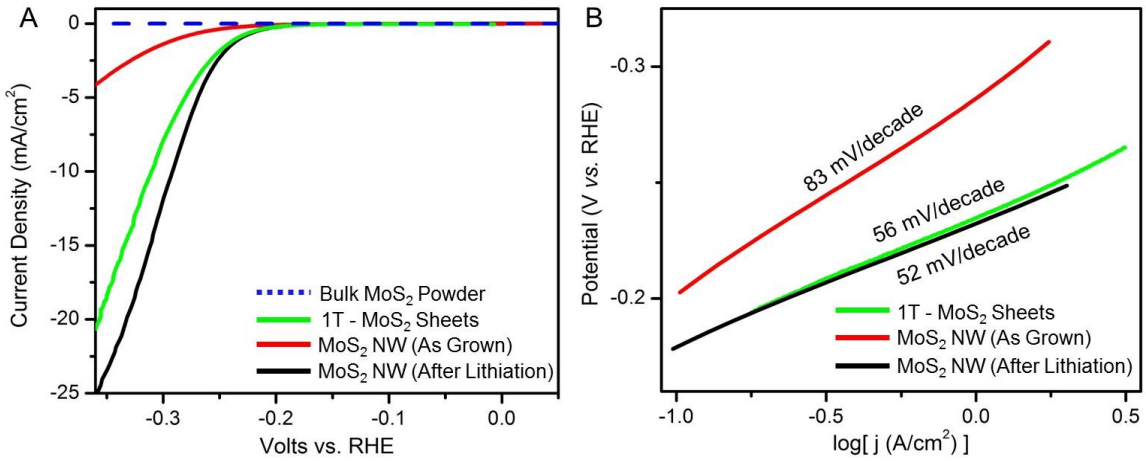

Figure 2. A) Linear sweep voltammograms showing the HER catalytic activity of MoS_2 nanowires, both as synthesized (red curve) and after lithiation (black curve). The HER activity for chemically exfoliated 1T-MoS_2 (green curve) 2D sheets is included for comparison. B) Tafel slopes of MoS_2 nanostructures. The HER activity for bulk MoS_2 powder (blue dotted curve) is shown in SI, as it is outside the range shown.

A 50 mV shift (from -0.2V to -0.15V vs. RHE) in the on-set potential (E_{onset}) was obtained for the nanowires following chemical intercalation, as seen in Figure 2A. Moreover, a significant six-fold increase in current density was observed, from ~4 mA/cm^2 to ~25

mA/cm^2 at -0.35 V. These results clearly indicate a significant enhancement in electrochemical activity upon chemical exfoliation. Bulk MoS_2 powder is also analyzed for catalytic activity in a similar manner. It shows an HER onset potential of ~ -0.8 V and a large Tafel slope of 156 mV/decade indicating extremely poor catalytic activity (Figure S4). For comparison, we also include the results from chemically exfoliated nanosheets forming the metallic 1T-MoS_2 (lithiated) sheets that show high HER activity due to phase transformation[14] with an onset potential of -0.15 V and Tafel slope of 52 mV/decade as seen in Figure 2A and B. Tafel slopes of all the catalysts are reported in Figure 2B to identify the mechanism of hydrogen evolution.

3.3 Reaction Pathways for Hydrogen Evolution

In order to determine the mechanism of hydrogen evolution at the electrode interface, detailed analysis of Tafel plots is performed to indicate the rate-limiting step. Typically, there are three elementary rate-determining reactions involved in HER at any catalyst surface. Specifically, the proton adsorption (known as the Volmer (eq. 1) step), followed by either (a) the evolution of molecular hydrogen by the combination of an adsorbed proton and a proton from solution (Heyrovsky (eq. 2) step), or (b) the combination of two adsorbed protons (Tafel (eq. 3) step.[49, 50] Two main pathways for hydrogen evolution are Volmer-Heyrovsky (1-2) or Volmer-Tafel (1-3).

Volmer: $H^+ + e^- \rightarrow H_{ads}$ (1)

Heyrovsky: $H_{ads} + H^+ + e^- \rightarrow H_2$ (2)

Tafel: $H_{ads} + H_{ads} \rightarrow H_2$ (3)

Experimental observation and kinetic modeling show that if the adsorption of a proton, *i.e.* the Volmer step, is the rate-determining step, then a Tafel slope of ~120 mV/decade should be

observed. However, if the evolution of molecular hydrogen is the rate-determining step, then a Tafel slope of ~40 mV/decade or ~30 mV/decade should be observed, indicative of the Heyrovsky or Tafel steps respectively.[8, 49, 50] It is important to understand that these values will only hold if the same rate-determining step is homogeneous throughout the catalyst. However, this is rarely the case. Multiple reactions occur at any given applied potential as a consequence of different reaction sites. Analysis of the change in Tafel slopes of the MoS_2 nanowires before and after lithiation (~90 and ~50 mV/decade) shows a change in the rate-determining step, shifting from adsorption limited to hydrogen evolution limited, suggesting the exposure of more adsorption sites (increase in active defect sites *vs.* relatively inactive basal plane).

As shown in Figure 1B, as-grown MoS_2 nanowires have a 5-10 nm highly oriented, single crystalline shell on the reduced oxide core. The relatively inert basal plane of 2H-MoS_2 is parallel to the nanowire length, so there are few edge sites exposed for hydrogen adsorption. After lithiation, a polycrystalline shell with random orientations and a higher concentration of more active defect sites is obtained as shown earlier (Figure 1D). Measurment of the double layer capacitance (Figure S6) *via* cyclic voltammetry at higher scan rates[51], show that the actual, wetted surface area of the nanowires does not change significantly following the lithium exfoliation; the increased catalysis is due predominantly to the exposure of active sites. These phenomena, *i.e.* increased exposure of defect sites for absorption and a conductive, high surface area architecture, explain the significantly improved onset potential and current density of the HER on exfoliated MoS_2 nanowires. Bulk MoS_2 powder has a Tafel slope of 156 mV/decade, and after lithium exfoliation, a 56 mV/decade Tafel slope is obtained for the 2D sheets; this significant improval in kinetics attributed to phase transformation.[14, 26]

3.4 Determination of Phase and Binding Energies of Synthesized Nanostructures

Although TEM imaging indicates different origins of catalytic behavior between the core-shell MoO_x/MoS_2 nanowires and the 2D exfoliated sheets, the exfoliated nanowires show similar Tafel slopes and catalytic performance, so further correlated Raman and XPS measurements are performed to understand the real origin of the catalysis in the nanowires.

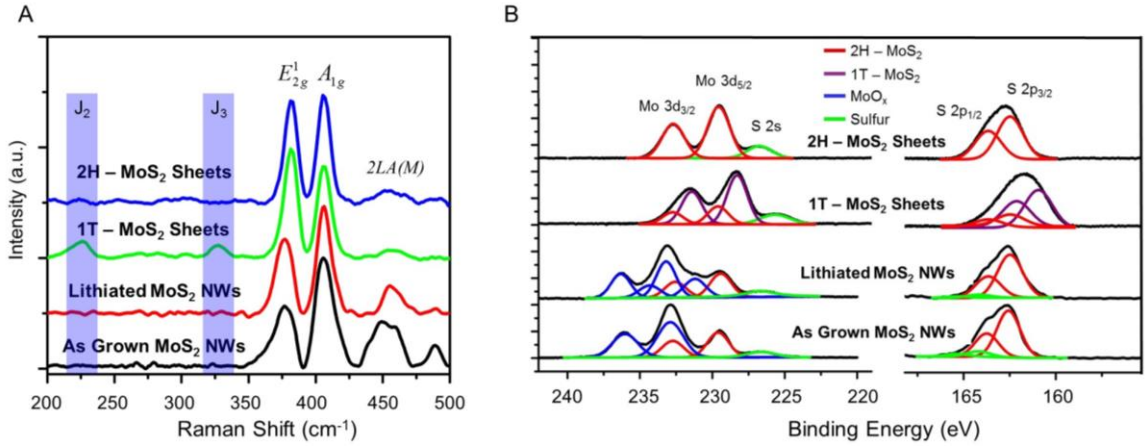

Figure 3. A) Raman spectroscopy of MoS_2 nanowire arrays before (black curve) and after lithiation (red curve), as well as chemically exfoliated 1T-MoS_2 sheets (green curve) and 2H-MoS_2 sheets (blue curve). The locations of the J_2 and J_3 for 1T-MoS_2 is shown by the shaded area. B) XPS spectra showing Mo 3d, S 2s, as well as the S 2p core level binding energy regions for MoS2 nanowire arrays both as grown and after chemical exfoliation. Chemically exfoliated 1T-MoS_2 sheets and 2H-MoS_2 sheet analysis is shown for comparison.

Raman spectroscopy (Figure 3A) is used to confirm the presence of the trigonal and octahedral phases. 2H-MoS_2 has two strong Raman peaks at ~382 and ~407 cm^{-1}, corresponding to the E^1_{2g} and A_{1g} respectively, as well as a broad peak at 454 cm^{-1}, which corresponds to two peaks, a second order zone-edge phonon peak 2LA(M) and a first order optical phonon peak, A_{2u}.[52, 53] The 1T phase has unique Raman vibrational peaks at ~220 (J_2) and ~325 cm^{-1} (J_3)[45] which are highlighted by the shaded area in Figure 3A and are clearly evident in the chemically exfoliated MoS_2 sheets (green curve). These vibrational modes are only active when the 1T phase is present. In comparison, Raman analysis of the MoS_2

nanowire arrays before (black curve) and after lithiation (red curve) show no evidence of any phase transformation from the 2H to the 1T phase. This provides strong evidence that the improved HER catalytic activity of the MoS_2 nanowires after lithiation is a result of the disorder caused by the intercalation, exposing more active defect sites for HER catalysis, rather than a crystal phase transformation.

XPS spectra of the nanowire samples are shown in Figure 3B. The as grown nanowires clearly show the trigonal prismatic 2H-MoS_2 shell on a reduced MoO_x core, with prominent peaks at ~229 and 232 eV, corresponding to Mo^{4+} $3d_{5/2}$ and Mo^{4+} $3d_{3/2}$ of 2H-MoS_2 respectively, denoted by the red curve. The strong peak at 232 eV is a convolution of the Mo^{4+} $3d_{3/2}$ from MoS_2 and the $3d_{5/2}$ of Mo^{6+} from the reduced molybdenum oxide (MoO_x) core, along with its corresponding doublet $3d_{3/2}$ at ~236 eV, denoted by the blue curve. 2H-MoS_2 has a characteristic doublet peak resulting from the anion for S $2p_{3/2}$ and S $2p_{1/2}$, which are seen at ~162.5 and ~163.7 eV respectively. The ratio of the relative intensities of the S 2p and Mo 3d peaks corresponding to 2H-MoS_2 leads to a S:Mo ratio of ~2:1, consistent with the expected elemental composition for MoS_2.

After lithiation of the nanowires, the ratio of XPS peak intensities corresponding to 2H-MoS_2 is not significantly altered, still maintaining a S:Mo ratio of ~2:1, indicating that the MoS_2 shell has not changed stoichiometry. Analysis of core level binding energies of sulfur 2p shows no change in energy. In the nanowire samples, there is a very weak sulfur peak at a higher binding energy, which denotes mild oxidation on the surface. XPS of the 1T octahedral phase MoS_2, indicated by the purple curve, shows a large (0.9 eV) shift of the Mo 3d binding energies and a corresponding shift and broadening of the S 2p energies.[13, 45, 54] This is clearly not the case in the lithiation of the core-shell MoO_x/MoS_2 nanowire arrays, which maintain the 2H-MoS_2 phase after lithium intercalation and any modification is due to changes in morphology of the nanowires. Analysis of the Mo 3d binding energies of the

nanowires after exfoliation shows an additional oxidation state, which suggests that the intercalated lithium interacts with the MoO_x core and starts to reduce it further.

A critical question still remains that why lithium intercalation of MoS_2 particles leads to a phase transition and formation of the 1T metallic phase, whereas the core-shell MoO_x/MoS_2 nanowires do not exhibit this phase transition following lithiation. During lithium intercalation of bulk MoS_2, lithium donates an electron to the crystal lattice, inducing a 60° strain leading to the phase transition from semiconducting 2H to the metastable metallic 1T phase.[13, 41, 55] However, the molybdenum and sulfur binding energies composing the MoS_2 shell of the core-shell nanowires are unaffected following exfoliation. The volume expansion during the intercalation leads to disruption of the nanowire shell, causing disorder and the creation of more active defect and crystal edge sites, but the original 2H-MoS_2 crystal structure is maintained. To further obtain the mechanistic origin of catalytic activity in structures, temperature dependent annealing studies were performed on both nanowires and nanosheets.

3.5 Insight into the Mechanism via Controlled Annealing Studies

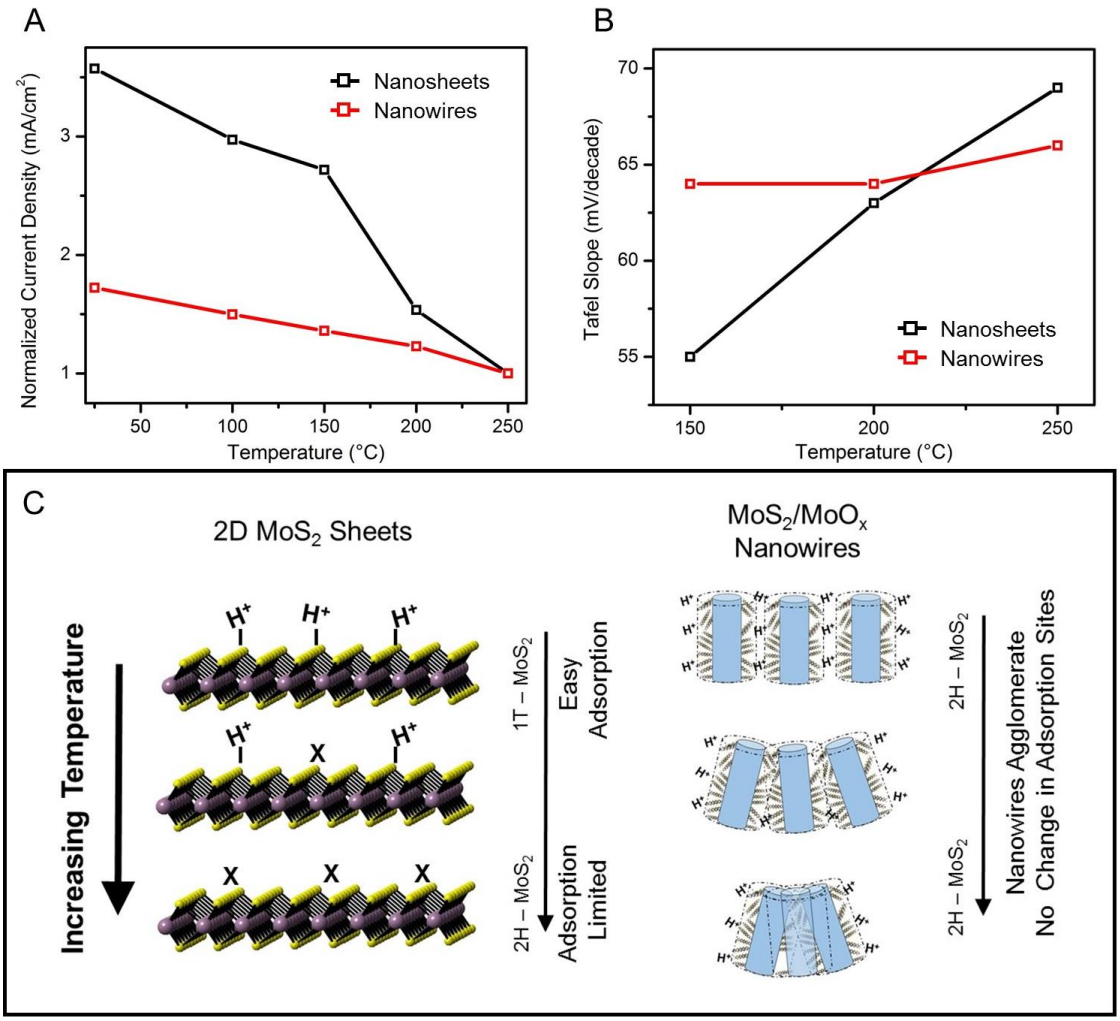

Figure 4. A) Current density (mA/cm^2) at -0.3 mV vs. RHE for nanowires (red curve) and nanosheets (black curve) as a function of annealing temperature. Current density was normalized with current density value at 250°C B) Comparison of Tafel slope of nanowires (red curve) and nanosheets (black curve) with increasing annealing temperatures. C) Schematic showing the morphology effects with increasing temperature: Crystal phase conversion in the 2D sheets and shift towards adsorption rate limited kinetics, whereas agglomeration of the nanowires is the reason for loss of minimal activity, with desorption as the rate-limiting step.

We performed step-by-step annealing and the subsequent electrochemical activity is measured to address the origin of catalytic activity. As shown in Figure 4A, a linear and

gradual decrease in the current density is observed for nanowires up to 250°C; whereas a sharp drop in current density is obtained for the exfoliated 2D sheets at 150°C, indicating the phase transformation from metallic 1T to semiconducting 2H.[45] No such phenomenon is observed for the annealed nanowires. A clearer indication is obtained from Tafel plots (Figure 4B); above 150°C no change in the Tafel slope is observed for the exfoliated nanowires, which remains constant (64 - 65 mV/decade from 150 to 250°C), indicating that the desorption of hydrogen remains the dominant rate limiting step and there is no change in catalytic sites during annealing. However, the Tafel slope for the 2D sheets increases from 54 to 70 mV/decade between annealing at 150°C and 250°C, indicating that hydrogen adsorption (Volmer) emerges as the rate limiting step and different sites are now contributing to the catalysis; further indicating a crystal transformation from the metastable 1T to 2H phase. The slight decrease in electrochemical activity in the exfoliated nanowires is possibly due to agglomeration or sintering of the wires, leading to decreased surface area, but there is no change in the catalytic active sites or the HER on-set potentials (Figure S7). Figure 4C shows a cartoon demonstrating the effects of annealing on the MoS_2 2D sheets compared to the lithium intercalated nanowires. This annealing experiment is further proof that the lithium intercalated MoO_x/MoS_2 core/shell nanowires did not undergo phase transition to form the 1T phase, but also helps demonstrate the thermal stability of these nanowires.

4. Conclusion

Here, we report the enhancement of HER catalytic activity of core-shell MoO_x/MoS_2 nanowires following chemical exfoliation. The rapid volume expansion, which occurs due to lithium intercalation, disrupts the ordered crystal structure, leading to random orientations and the exposure of more catalytically active defect sites, a combination of increased quantity and increased activity of those defect sites. These defect sites are supported on a high surface area, conductive reduced molybdenum oxide nanowire, which results in improved charge transfer characteristics. This leads to a 50 mV improvement in the HER onset potential, as

well as a 600% increase in the generated current density at -0.35 V vs. RHE. Furthermore, Raman, XPS, and controlled annealing studies corroborate that the increased catalytic activity in the nanowires does not result from the formation of the metastable 1T-MoS_2 phase, which is typically formed by lithium exfoliation of bulk MoS_2 particles, but from the exposure of higher catalytically active surface area of the stable 2H-MoS_2 phase. The decrease in Tafel slope after lithiation experimentally confirms that more sites for hydrogen absorption, *i.e.* edge and defect sites, are exposed during the disruption of the MoS_2 shell. The thermal stability of the exfoliated nanowires, compared to the 1T MoS_2 sheets following annealing, is further confirmation of the different mechanisms of catalysis in the two architectures. This is the one of the first reports on the effects of intercalating lithium into core-shell chalcogenide nanowires, as well as one of the first investigations of the crystallographic effects of lithium intercalation on 1D nanowire morphologies.

Supporting Information

Schematic showing MoS_2 core-shell nanowire synthesis scheme. XRD patterns of bare MoO_3 nanowire array and MoO_3/MoS_2 core-shell nanowires. Electron Energy Loss Spectra (EELS) of the lithium intercalated MoS_2 nanowires. Details of crystallographic characterization techniques. Nyquist plot for series resistance in electrochemical testing. Electrocatalytic testing of bulk MoS_2 powder. Results of incremental lithiation. Double layer capacitance measurements of nanowires and 2D sheets. Effects of annealing of nanowires and nanosheets. This material is available free of charge via the Internet at http://pubs.acs.org.

Acknowledgements

The authors would like to acknowledge Center for Integrated Nanotechnologies and LDRD Funding at Los Alamos National Laboratory, as well as the Conn Center for Renewable Energy Research at the University of Louisville for facilities and access to characterization equipment. Development of samples and characterization was supported partially by DOE

EPSCoR (DE-FG02-07ER46375) and by a graduate fellowship funded by NASA Kentucky under NASA award No: NNX10AL96H.

References.

1. Rostrup-Nielsen, J. R.; Sehested, J.; Norskov, J. K. Hydrogen and Synthesis Gas By Steam and CO2 Reforming. In *Advances in Catalysis*, Gates, B. C.; Knozinger, H., Eds. 2002; Vol. 47, pp 65-139.

2. Cortright, R. D.; Davda, R. R.; Dumesic, J. A. Hydrogen from Catalytic Reforming of Biomass-Derived Hydrocarbons in Liquid Water. *Nature* **2002**, *418*, 964-967.

3. Ashcroft, A. T.; Cheetham, A. K.; Green, M. L. H.; Vernon, P. D. F. Partial Oxidation of Methane to Synthesis Gas-Using Carbon-Dioxide. *Nature* **1991**, *352*, 225-226.

4. Rossmeisl, J.; Logadottir, A.; Norskov, J. K. Electrolysis of Water on (Oxidized) Metal Surfaces. *Chem. Phys.* **2005**, *319*, 178-184.

5. Khaselev, O.; Turner, J. A. A Monolithic Photovoltaic-Photoelectrochemical Device for Hydrogen Production Via Water Splitting. *Science* **1998**, *280*, 425-427.

6. Joo, S. H.; Choi, S. J.; Oh, I.; Kwak, J.; Liu, Z.; Terasaki, O.; Ryoo, R. Ordered Nanoporous Arrays of Carbon Supporting High Dispersions of Platinum Nanoparticles. *Nature* **2001**, *412*, 169-172.

7. Si, Y. C.; Samulski, E. T. Exfoliated Graphene Separated by Platinum Nanoparticles. *Chem. Mater.* **2008**, *20*, 6792-6797.

8. Sheng, W. C.; Gasteiger, H. A.; Shao-Horn, Y. Hydrogen Oxidation and Evolution Reaction Kinetics on Platinum: Acid vs Alkaline Electrolytes. *J. Electrochem. Soc.* **2010**, *157*, B1529-B1536.

9. Li, H.-H.; Ma, S.-Y.; Fu, Q.-Q.; Liu, X.-J.; Wu, L.; Yu, S.-H. Scalable Bromide-Triggered Synthesis of Pd@Pt Core-Shell Ultrathin Nanowires with Enhanced Electrocatalytic Performance toward Oxygen Reduction Reaction. *J. Am. Chem. Soc.* **2015**, *137*, 7862-7868.

10. Ho, W. K.; Yu, J. C.; Lin, J.; Yu, J. G.; Li, P. S. Preparation and Photocatalytic Behavior of MoS2 and WS2 Nanocluster Sensitized TiO2. *Langmuir* **2004**, *20*, 5865-5869.

11. King, L. A.; Zhao, W.; Chhowalla, M.; Riley, D. J.; Eda, G. Photoelectrochemical Properties of Chemically Exfoliated MoS2. *J. Mater. Chem. A* **2013**, *1*, 8935-8941.

12. Jing, D. W.; Guo, L. J. WS2 Sensitized Mesoporous TiO2 for Efficient Photocatalytic Hydrogen Production from Water Under Visible Light Irradiation. *Catal. Commun.* **2007**, *8*, 795-799.

13. Chhowalla, M.; Shin, H. S.; Eda, G.; Li, L.-J.; Loh, K. P.; Zhang, H. The Chemistry of Two-Dimensional Layered Transition Metal Dichalcogenide Nanosheets. *Nature Chem.* **2013**, *5*, 263-275.

14. Voiry, D.; Salehi, M.; Silva, R.; Fujita, T.; Chen, M.; Asefa, T.; Shenoy, V. B.; Eda, G.; Chhowalla, M. Conducting MoS2 Nanosheets as Catalysts for Hydrogen Evolution Reaction. *Nano Lett.* **2013**, *13*, 6222-6227.

15. Voiry, D.; Yamaguchi, H.; Li, J. W.; Silva, R.; Alves, D. C. B.; Fujita, T.; Chen, M. W.; Asefa, T.; Shenoy, V. B.; Eda, G., et al. Enhanced Catalytic Activity in Strained Chemically Exfoliated WS2 Nanosheets for Hydrogen Evolution. *Nat. Mater.* **2013**, *12*, 850-855.

16. Hinnemann, B.; Moses, P. G.; Bonde, J.; Jorgensen, K. P.; Nielsen, J. H.; Horch, S.; Chorkendorff, I.; Norskov, J. K. Biornimetic Hydrogen Evolution: MoS2 Nanoparticles as Catalyst for Hydrogen Evolution. *J. Am. Chem. Soc.* **2005**, *127*, 5308-5309.

17. Chen, Z.; Cummins, D.; Reinecke, B. N.; Clark, E.; Sunkara, M. K.; Jaramillo, T. F. Core-shell MoO3-MoS2 Nanowires for Hydrogen Evolution: A Functional Design for Electrocatalytic Materials. *Nano Lett.* **2011**, *11*, 4168-4175.

18. Jaramillo, T. F.; Jorgensen, K. P.; Bonde, J.; Nielsen, J. H.; Horch, S.; Chorkendorff, I. Identification of Active Edge Sites for Electrochemical H-2 Evolution From MoS2 Nanocatalysts. *Science* **2007**, *317*, 100-102.

19. Kibsgaard, J.; Chen, Z. B.; Reinecke, B. N.; Jaramillo, T. F. Engineering the Surface Structure of MoS2 to Preferentially Expose Active Edge Sites for Electrocatalysis. *Nat. Mater.* **2012**, *11*, 963-969.

20. Benck, J. D.; Hellstern, T. R.; Kibsgaard, J.; Chakthranont, P.; Jaramillo, T. F. Catalyzing the Hydrogen Evolution Reaction (HER) with Molybdenum Sulfide Nanomaterials. *ACS Catal.* **2014**, *4*, 3957-3971.

21. Benck, J. D.; Chen, Z. B.; Kuritzky, L. Y.; Forman, A. J.; Jaramillo, T. F. Amorphous Molybdenum Sulfide Catalysts for Electrochemical Hydrogen Production: Insights into the Origin of their Catalytic Activity. *ACS Catal.* **2012**, *2*, 1916-1923.

22. Li, Y.; Wang, H.; Xie, L.; Liang, Y.; Hong, G.; Dai, H. MoS2 Nanoparticles Grown on Graphene: An Advanced Catalyst for the Hydrogen Evolution Reaction. *J. Am. Chem. Soc.* **2011**, *133*, 7296-7299.

23. Wang, H. T.; Lu, Z. Y.; Kong, D. S.; Sun, J.; Hymel, T. M.; Cui, Y. Electrochemical Tuning of MoS2 Nanoparticles on Three-Dimensional Substrate for Efficient Hydrogen Evolution. *ACS Nano* **2014**, *8*, 4940-4947.

24. Kong, D. S.; Wang, H. T.; Cha, J. J.; Pasta, M.; Koski, K. J.; Yao, J.; Cui, Y. Synthesis of MoS2 and MoSe2 Films with Vertically Aligned Layers. *Nano Lett.* **2013**, *13*, 1341-1347.

25. Wu, Z. Z.; Fang, B. Z.; Wang, Z. P.; Wang, C. L.; Liu, Z. H.; Liu, F. Y.; Wang, W.; Alfantazi, A.; Wang, D. Z.; Wilkinson, D. P. MoS2 Nanosheets: A Designed Structure with High Active Site Density for the Hydrogen Evolution Reaction. *ACS Catal.* **2013**, *3*, 2101-2107.

26. Wang, H. T.; Lu, Z. Y.; Xu, S. C.; Kong, D. S.; Cha, J. J.; Zheng, G. Y.; Hsu, P. C.; Yan, K.; Bradshaw, D.; Prinz, F. B., et al. Electrochemical Tuning of Vertically Aligned MoS2 Nanofilms and Its Application in Improving Hydrogen Evolution Reaction. *Proc. Nat. Acad. Sci. U.S.A.* **2013**, *110*, 19701-19706.

27. Lukowski, M. A.; Daniel, A. S.; Meng, F.; Forticaux, A.; Li, L. S.; Jin, S. Enhanced Hydrogen Evolution Catalysis from Chemically Exfoliated Metallic MoS2 Nanosheets. *J. Am. Chem. Soc.* **2013**, *135*, 10274-10277.

28. Lukowski, M. A.; Daniel, A. S.; English, C. R.; Meng, F.; Forticaux, A.; Hamers, R. J.; Jin, S. Highly Active Hydrogen Evolution Catalysis from Metallic WS2 Nanosheets. *Energy Environ. Sci.* **2014**, *7*, 2608-2613.

29. Tsai, C.; Abild-Pedersen, F.; Norskov, J. K. Tuning the MoS2 Edge-Site Activity for Hydrogen Evolution via Support Interactions. *Nano Lett.* **2014**, *14*, 1381-1387.

30. Wang, T. Y.; Liu, L.; Zhu, Z. W.; Papakonstantinou, P.; Hu, J. B.; Liu, H. Y.; Li, M. X. Enhanced Electrocatalytic Activity for Hydrogen Evolution Reaction from Self-Assembled Monodispersed Molybdenum Sulfide Nanoparticles on an Au Electrode. *Energy Environ. Sci.* **2013**, *6*, 625-633.

31. Yun-Fei, X.; Min-Rui, G.; Ya-Rong, Z.; Jun, J.; Shu-Hong, Y. Nickel/Nickel(II) Oxide Nanoparticles Anchored onto Cobalt(IV) Diselenide Nanobelts for the Electrochemical Production of Hydrogen. *Angew. Chem. Int. Ed.* **2013**, *52*, 8546-50.

32. Daage, M.; Chianelli, R. R. Structure-Function Relations in Molybdenum Sulfide Catalysts - The Rim-Edge Model. *J. Catal.* **1994**, *149*, 414-427.

33. Gao, M. R.; Liang, J. X.; Zheng, Y.; Xu, Y.; Jiang, J.; Gao, Q.; Li, J.; Yu, S. H. An Efficient Molybdenum Disulfide/ Cobalt Diselenide Hydrid Catalyst for Electrochemical Hydrogen Generation. *Nature Comm.* **2015**, *6*, 5982.

34. Chianelli, R. R.; Ruppert, A. F.; Behal, S. K.; Kear, B. H.; Wold, A.; Kershaw, R. The Reactivity of MoS2 Single-Crystal Edge Planes. *J. Catal.* **1985**, *92*, 56-63.

35. Bollinger, M. V.; Lauritsen, J. V.; Jacobsen, K. W.; Norskov, J. K.; Helveg, S.; Besenbacher, F. One-Dimensional Metallic Edge States in MoS2. *Phys. Rev. Lett.* **2001**, *87*.

36. Raybaud, P.; Hafner, J.; Kresse, G.; Kasztelan, S.; Toulhoat, H. Structure, Energetics, and Electronic Properties of the Surface of a Promoted MoS2 Catalyst: an Ab Initio Local Density Functional Study. *J. Catal.* **2000**, *190*, 128-143.

37. Raybaud, P.; Hafner, J.; Kresse, G.; Kasztelan, S.; Toulhoat, H. Ab Initio Study of the H2-H2S/MoS2 Gas-Solid Interface: the Nature of the Catalytically Active Sites. *J. Catal.* **2000**, *189*, 129-146.

38. Coehoorn, R.; Haas, C.; Dijkstra, J.; Flipse, C. J. F.; Degroot, R. A.; Wold, A. Electronic-Structure of MoSe2, MoS2, and WSe2 .1. Band-Structure Calculations and Photoelectron-Spectroscopy. *Phys. Rev. B* **1987**, *35*, 6195-6202.

39. Coleman, J. N.; Lotya, M.; O'Neill, A.; Bergin, S. D.; King, P. J.; Khan, U.; Young, K.; Gaucher, A.; De, S.; Smith, R. J., et al. Two-Dimensional Nanosheets Produced by Liquid Exfoliation of Layered Materials. *Science* **2011**, *331*, 568-571.

40. Mak, K. F.; Lee, C.; Hone, J.; Shan, J.; Heinz, T. F. Atomically Thin MoS2: A New Direct-Gap Semiconductor. *Phys. Rev. Lett.* **2010**, *105*.

41. Py, M. A.; Haering, R. R. Structural Destabilization Induced by Lithium Iintercalation in MoS2 and Related-Compounds. *Can. J. Phys.* **1983**, *61*, 76-84.

42. Joensen, P.; Frindt, R. F.; Morrison, S. R. Single-Layer MoS2. *Mater. Res. Bull.* **1986**, *21*, 457-461.

43. Matte, H.; Gomathi, A.; Manna, A. K.; Late, D. J.; Datta, R.; Pati, S. K.; Rao, C. N. R. MoS2 and WS2 Analogues of Graphene. *Angew. Chem. Int. Ed.* **2010**, *49*, 4059-4062.

44. Eda, G.; Fujita, T.; Yamaguchi, H.; Voiry, D.; Chen, M.; Chhowalla, M. Coherent Atomic and Electronic Heterostructures of Single-Layer MoS2. *ACS Nano* **2012**, *6*, 7311-7317.

45. Eda, G.; Yamaguchi, H.; Voiry, D.; Fujita, T.; Chen, M.; Chhowalla, M. Photoluminescence from Chemically Exfoliated MoS2. *Nano Lett.* **2011**, *11*, 5111-5116.

46. Ebner, M.; Marone, F.; Stampanoni, M.; Wood, V. Visualization and Quantification of Electrochemical and Mechanical Degradation in Li Ion Batteries. *Science* **2013**, *342*, 716-720.

47. Winter, M.; Wrodnigg, G. H.; Besenhard, J. O.; Biberacher, W.; Novak, P. Dilatometric Investigations of Graphite Electrodes in Nonaqueous Lithium Battery Electrolytes. *J. Electrochem. Soc.* **2000**, *147*, 2427-2431.

48. Cummins, D. R. Synthesis of Molybdenum Oxide Nanowires and Their Facile Conversion to Molybdenum Sulfide. 'Thesis', University of Louisville, Louisville, KY, 2009.

49. Pentland, N.; Bockris, J. O.; Sheldon, E. Hydrogen Evolution Reaction on Copper, Gold, Molybdenum, Palladium, Rhodium, and Iron. *J. Electrochem. Soc.* **1957**, *104*, 182-194.

50. Conway, B. E.; Tilak, B. V. Interfacial Processes Involving Electrocatalytic Evolution and Oxidation of H2, and the Role of Chemisorbed H. *Electrochim. Acta* **2002**, *47*, 3571-3594.

51. Faber, M. S.; Dziedzic, R.; Lukowski, M. A.; Kaiser, N. S.; Ding, Q.; Jin, S. High Performance Electrocatalysis Using Metallic Cobalt Pyrite (CoS2) Micro- and Nanostructures. *J. Am. Chem. Soc.* **2014**, *136*, 10053-10061.

52. Li, H.; Zhang, Q.; Yap, C. C. R.; Tay, B. K.; Edwin, T. H. T.; Olivier, A.; Baillargeat, D. From Bulk to Monolayer MoS2: Evolution of Raman Scattering. *Adv. Funct. Mater.* **2012**, *22*, 1385-1390.

53. Frey, G. L.; Tenne, R.; Matthews, M. J.; Dresselhaus, M. S.; Dresselhaus, G. Raman and Resonance Raman Investigation of MoS2 Nanoparticles. *Phys. Rev. B* **1999**, *60*, 2883-2892.

54. Papageorgopoulos, C. A.; Jaegermann, W. Li Intercalation Across and Along the Van-der-Waals Surfaces of MoS2(0001). *Surf. Sci.* **1995**, *338*, 83-93.

55. Heising, J.; Kanatzidis, M. G. Structure of restacked MoS2 and WS2 elucidated by electron crystallography. *J. Am. Chem. Soc.* **1999**, *121*, 638-643.

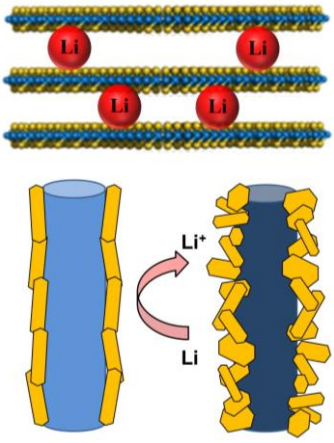

Table of Contents Figure